

Ellipsometric determination of universal critical adsorption scaling functions

J. H. Carpenter, J.-H. J. Cho, and B. M. Law

Condensed Matter Laboratory, Department of Physics, Kansas State University, Manhattan, Kansas 66506-2601

(Received 10 May 1999)

In this paper we determine and compare a number of theoretical models which describe the universal scaling functions for critical adsorption in the strong surface field limit. The $P1$ and $P3$ models, which are continuous up to and including the first and third derivatives, respectively, provide excellent descriptions of the ellipsometric data for four different critical binary liquid mixtures. The exponential-Padé model, initially proposed by Liu and Fisher [Phys. Rev. A **40**, 7202 (1989)], provides a reasonable but less accurate description of the one-phase experimental data. This later model has the advantage, however, that it is continuous in all derivatives.

PACS number(s): 68.35.Rh, 68.10.-m, 64.60.Fr, 82.65.Dp

I. INTRODUCTION

At the liquid/vapor or liquid/solid interface of a binary liquid mixture, the liquid component with the lowest surface free energy will adsorb at the surface, in preference to the other component. This preferential adsorption is found even in the two-phase region of the liquid mixture provided a wetting layer does not form [1]. It is important to obtain a quantitative understanding of adsorption because it influences the interactions between colloidal particles [2] and is important in fluid flow through porous media [3].

Twenty years ago Fisher and de Gennes (FdG) [4] predicted that this preferential adsorption would acquire very interesting universal properties near a *critical point* of the binary liquid mixture. In their scaling theory, the adsorption is governed by a surface field, h_1 , and the adsorption structure in the vicinity of the surface is correlated over a distance of the order of the bulk correlation length, $\xi_{\pm} = \xi_{o\pm} t^{-\nu}$, where the reduced temperature $t = |T_c - T|/T_c$, ν ($=0.632$ [5]) is a bulk critical exponent, $\xi_{o\pm}$ is a system-dependent amplitude, and throughout this publication the subscript $+$ ($-$) refers to the one- (two-) phase region of the liquid mixture. The distance over which the adsorption structure is correlated obviously diverges as the critical temperature T_c is approached. In [4], the local adsorption at a distance z (≥ 0) from the surface (at $z=0$) is governed by the local order parameter $m(z,t)$, where

$$m_{\pm}(z,t) = M_{-} t^{\beta} G_{\pm}[(z+z_e)/\xi_{\pm}, h_1 t^{-\Delta_1}], \quad (1)$$

Δ_1 (≈ 0.5 [6]) and β ($=0.328$ [5]) are critical exponents, the term $M_{-} t^{\beta}$ describes the shape of the coexistence curve for the binary liquid mixture, while the function $G_{\pm}(x,y)$ is predicted to be *universal* with differing forms in the one- and two-phase regions. The system-dependent extrapolation length z_e is discussed in more detail in Sec. IV. In critical binary liquid mixtures, the order parameter in the bulk at $z = \infty$, namely $m(\infty,t)$, is frequently taken as the volume fraction of one of the components because this usually provides the most symmetric coexistence curve [7]. A reasonable assumption, therefore, is that the volume fraction also serves as the appropriate order parameter in the vicinity of a surface so that

$$m(z,t) = \varphi_L(z,t) - \varphi_L(+\infty,0), \quad (2)$$

where $\varphi_L(z,t)$ is the local volume fraction of the lower-density liquid component (L) and $\varphi_L(+\infty,0)$ represents the corresponding critical volume fraction. The functional forms for $G_{\pm}(x,y)$ are not well understood, although some theoretical progress has been made recently [8]. Only one experiment has examined the dependence of the adsorption upon the surface field h_1 [9]. In this paper we are mainly interested in a limiting case of this function, for *strong* h_1 fields, where sufficiently close to T_c the first few layers at the liquid/vapor surface are completely saturated with the preferred component and Eq. (1) simplifies to

$$m_{\pm}(z,t) = M_{-} t^{\beta} P_{\pm}[(z+z_e)/\xi_{\pm}], \quad (3)$$

where $P_{\pm}(x) \equiv P_{\pm} = G_{\pm}(x,\infty)$ is again a *universal* function which takes differing forms in the one- and two-phase regions. In this simpler situation, which is believed to occur most frequently in nature, $P_{\pm}(x)$ is predicted to exhibit power-law decay [Eq. (5) below] at small x ($\ll 1$), which crosses over to an exponential decay [Eq. (7) below] at large x ($\gg 1$). Various forms for the crossover from small x to large x have been proposed. Liu and Fisher [10] suggested a number of different *Ansätze* which incorporate the appropriate asymptotic behavior. Diehl and Smock [11] have deduced renormalization-group theory (RG) estimates for P_{\pm} to order ϵ while Smock, Diehl, and Landau [12] have obtained estimates from Monte Carlo simulations (MC).

A large variety of experimental techniques have been used to study critical adsorption including volumetry [13], evanescent-wave light scattering [14], optical reflectometry [15], ellipsometry [16–18], and neutron reflectometry [19,20]. Unfortunately, none of these techniques directly measures the universal function P_{\pm} . Instead, various integrals over P_{\pm} are measured and therefore it is much more difficult to extract the precise functional forms for P_{\pm} from experimental data. Two neutron reflectometry experiments [19,20] have confirmed the power-law behavior of $P_{+}(x)$ at small x , while ellipsometry and optical reflectometry experiments have measured various integrals over $P_{\pm}(x)$ [15,21], obtained evidence for the z/ξ dependence of $P_{\pm}(x)$, and enabled the extraction of various universal parameters re-

lated to the form of $P_{\pm}(x)$ [10,22,23]. The RG and MC estimates for $P_{\pm}(x)$ provide a reasonable qualitative description for a number of ellipsometric critical adsorption experiments [22,24], while a novel comparison between theory and experiment has even managed to determine estimates of $P_{+}(x)$ for several different liquid mixtures [23]; however, at intermediate values of $x(\sim 1)$ these functional forms differ by more than 100% and therefore these experimental determinations of $P_{+}(x)$ cannot be claimed to fulfill the universality requirement of $P_{+}(x)$. This is an unsatisfactory situation because $P_{\pm}(x)$ are limiting functions for other more complicated situations near the critical point of the liquid mixture. For example, (i) the form of $G_{\pm}(x,y)$ can obviously never be quantitatively understood until the simpler function $P_{\pm}(x)$ is determined precisely, (ii) finite-size effects in critical films [25] cannot readily be understood until the semi-infinite system, where $P_{\pm}(x)$ is applicable, has been determined, and (iii) geometric effects (e.g., adsorption around spherical colloidal particles [26]) cannot be understood until planar surfaces are understood. The purpose of this paper is therefore to accurately determine and compare various models for the universal functions $P_{\pm}(x)$ with the ellipsometric data of four different critical binary liquid mixtures. A preliminary account of this work has been previously published in [24].

This paper is set out as follows. The general theoretical behavior for $P_{\pm}(x)$ is discussed in Sec. II. We are mainly interested in the determination of $P_{\pm}(x)$ from ellipsometric data, therefore in Sec. III we provide a detailed discussion of what precisely has been previously determined from ellipsometric measurements of critical adsorption. In Sec. IV, we present a number of theoretical models for $P_{\pm}(x)$ which conform with the general theoretical behavior of Sec. II and discuss the general methodology for determining $P_{\pm}(x)$ from ellipsometric data. We apply this methodology for the determination of $P_{\pm}(x)$ in Sec. V, where the specific details are relegated to an Appendix. This paper concludes with a summary and discussion of our results in Sec. VI.

II. THEORY

According to our definition for the local order parameter $m(z,t)$ [Eq. (2)], the universal surface scaling functions $P_{\pm}(x)$ [Eq. (3)] must take the limiting forms

$$P_{+}(\infty)=0 \quad \text{and} \quad P_{-}(\infty)=1 \quad (4)$$

in the bulk liquid so that the order parameter is either zero or describes the coexistence curve in, respectively, the one- or two-phase regions.

At criticality ($t=0$), we expect the adsorption to remain finite (and nonzero) so that $m(z,0)$ must lose its dependence upon the reduced temperature t ; this requirement implies that the small $x(\ll 1)$ behavior for the surface scaling function must be [4]

$$P_{\pm}(x) \cong c_{\pm} x^{-\beta/\nu}, \quad (5)$$

where c_{+} and c_{-} are universal numbers. At the critical temperature T_c , for second-order phase transitions, the local order parameter $m(z,t)$ is required to be continuous with an

analytic background with respect to the reduced temperature t at $t=0$, hence, from Eq. (5) [11],

$$\frac{c_{+}}{c_{-}} = \left(\frac{\xi_{0+}}{\xi_{0-}} \right)^{-\beta/\nu}, \quad (6)$$

where the correlation length amplitudes have a universal ratio $R_{\xi} = \xi_{0+}/\xi_{0-}$ whose value may depend upon whether the ratio R_{ξ} corresponds to the ‘‘true correlation length’’ or the ‘‘second moment of the bulk correlation length’’ [23]. For the true correlation length, Tarko and Fisher [27] determined that $R_{\xi} = 1.92$ while more recently Flöter and Dietrich used an interpolation scheme to estimate R_{ξ} in three dimensions from exact results in two and four dimensions; they found $R_{\xi} = 1.73 \pm 0.04$ [23]. For the second moment of the bulk correlation length, there is less uncertainty in this universal ratio; Liu and Fisher find that $R_{\xi} = 1.96 \pm 0.01$ [28], Monte Carlo simulations yield $R_{\xi} = 2.06 \pm 0.01$ [29], while Flöter and Dietrich determined that $R_{\xi} = 1.93 \pm 0.05$ [23]. The analysis of critical adsorption data in Sec. V will allow us to study this ratio. We will consider two values: $R_{\xi} = 1.96$, which agrees with many of the estimates above (independent of the definition for the correlation length), and the alternative $R_{\xi} = 1.73$ suggested by Flöter and Dietrich [23] for the true correlation length.

At large $x(\gg 1)$, the P_{\pm} function obeys the following asymptotic limit:

$$P_{\pm}(x) - P_{\pm}(\infty) \cong P_{\infty\pm} e^{-x}, \quad (7)$$

where $P_{\infty\pm}$ are universal numbers and the values for $P_{\pm}(\infty)$ are given in Eq. (4).

Equations (5) and (7) represent only the first terms in an asymptotic expansion. For the $x \rightarrow 0$ limit, Diehl and Smock [11] proposed the following expansion for the scaling function:

$$P_{\pm}(x) = c_{\pm} x^{-\beta/\nu} + c_{1\pm} x^{(1-\beta)/\nu} + c_{2\pm} x^{(2-\beta)/\nu} + c_{3\pm} x^{3-(\beta/\nu)} + \dots, \quad (8)$$

where $c_{1\pm}$, $c_{2\pm}$, etc. are additional universal numbers. This small x expansion follows from the requirement that the order parameter $m(z,t)$, immediately adjacent to the interface (for fixed $z \ll \xi$), exhibit the correct reduced temperature dependence as described in [11]. The fourth term in Eq. (8), namely $x^{3-(\beta/\nu)}$, exhibits a differing power-law dependence compared with the preceding terms; this originates from a $|t|^{2-\alpha}$ surface order-parameter singularity which is identical to that occurring in the bulk free energy [30], where α is the specific-heat critical exponent. From the analyticity of the analytic background at $t=0$ pairs of parameters, c_{1+} and c_{1-} are also related to each other through the ratio R_{ξ} [11] in analogy to Eq. (6); specifically [31]

$$\frac{c_{1+}}{c_{1-}} = - \left(\frac{\xi_{0+}}{\xi_{0-}} \right)^{(1-\beta)/\nu} \quad \text{and} \quad \frac{c_{2+}}{c_{2-}} = \left(\frac{\xi_{0+}}{\xi_{0-}} \right)^{(2-\beta)/\nu}. \quad (9)$$

For the $x \rightarrow \infty$ limit, Liu and Fisher [10] suggest that the more general asymptotic expansion

$$P_{\pm}(x) = P_{\pm}(\infty) + P_{\infty\pm} e^{-x} + P_{1\pm} e^{-2x} + P_{2\pm} e^{-3x} + \dots \quad (10)$$

should be valid where $P_{1\pm}$, $P_{2\pm}$, etc. are additional universal numbers. Smock, Diehl, and Landau [12] have deduced explicit RG expressions for the parameters $P_{\infty\pm}$, P_{1+} , and P_{2+} accurate to order ϵ .

III. ELLIPSOMETRIC MEASUREMENTS OF CRITICAL ADSORPTION

Ellipsometry is the most sensitive visible-wavelength optical technique for studying critical adsorption [32]. Essentially all of the ellipsometric measurements for critical adsorption have been conducted at the Brewster angle (θ_B) where the real component of the optical signal $\text{Re}(r_p/r_s)|_{\theta_B} = 0$, while the imaginary component or ellipticity is described by the Drude equation [35]

$$\begin{aligned} \bar{\rho}(t) &= \text{Im}(r_p/r_s)|_{\theta_B} \\ &= \frac{\pi}{\lambda} \frac{\sqrt{\epsilon_1 + \epsilon_2}}{\epsilon_1 - \epsilon_2} \int_{-\infty}^{\infty} \frac{[\epsilon(z,t) - \epsilon_1][\epsilon(z,t) - \epsilon_2]}{\epsilon(z,t)} dz \end{aligned} \quad (11)$$

in the limit of thin-film thicknesses compared with the wavelength of light, λ . [For our situation, Eq. (11) typically holds for $\xi < 20$ nm.] In this equation r_p and r_s are, respectively, the complex reflection amplitudes for polarizations parallel (p) and perpendicular (s) to the plane of incidence while $\epsilon(z,t)$ describes the variation of the optical dielectric constant from a value of ϵ_1 in the incident medium at $z = -\infty$ to a value of ϵ_2 in the substrate at $z = +\infty$. If the interface is rough or anisotropic, then the equation for the ellipticity needs to be supplemented or modified [32–34]. For sufficiently large correlation lengths ξ , close to T_c , the Drude equation is no longer valid and the ellipticity $\bar{\rho}$ must be determined by numerically solving Maxwell's equations using a particular model for $\epsilon(z,t)$ [36,37].

In many prior studies of critical adsorption, it has frequently been assumed that the dielectric profile $\epsilon(z,t)$ serves as the local order parameter. Flöter and Dietrich [23] discuss how to determine the universal number c_+ [Eq. (5)] and obtain estimates of the universal functions $P_{\pm}(x)$ from these dielectric profiles. We have used an alternative approach. The dielectric profile $\epsilon(z,t)$, required in the determination of the ellipticity $\bar{\rho}$, is related to the volume fraction profile $\varphi_L(z,t)$ via the two-component Clausius-Mossotti equation [38]

$$f(\epsilon) = \Omega[\varphi_L f(\epsilon_L) + (1 - \varphi_L)f(\epsilon_H)], \quad (12)$$

where

$$f(X) = \frac{X - 1}{X + 2}, \quad (13)$$

ϵ_L (ϵ_H) is the optical dielectric constant for the lighter (heavier) liquid component, and $\Omega = (V_A + V_B)/V_{A+B}$ is the volume ratio before mixing an AB liquid mixture ($V_A + V_B$) compared with after mixing this mixture (V_{A+B}). Throughout this paper we assume that there is negligible volume change on mixing so that $\Omega = 1$; typically Ω pro-

vides only an $\sim 2\%$ correction [38]. The volume fraction profile $\varphi_L(z,t)$ is then related to the local order parameter $m(z,t)$ and theoretical models for $P_{\pm}(x)$ through Eqs. (2) and (3). Smith and Law [39] have used this approach to demonstrate that the Drude equation [Eq. (11)] reduces to

$$\bar{\rho}(t) \sim t^{\beta-\nu} \int_0^{\infty} [P_{\pm}(x) - P_{\pm}(\infty)] dx + \bar{\rho}_{\text{BG}}(t) \quad (14)$$

to a good approximation for critical adsorption. The divergent $t^{\beta-\nu}$ term (originating from the critical portion of the interface for $z \geq 0$) dominates the weakly temperature-dependent background term $\bar{\rho}_{\text{BG}}(t)$ which includes contributions from the variation of the volume fraction on the vapor side of the interface [39] and from capillary wave fluctuations [21]. In [21], Eq. (14) was used to determine the universal integrals

$$\int_0^{\infty} P_+ \equiv \int_0^{\infty} P_+(x) dx = 1.97 \pm 0.08 \quad (15)$$

and

$$\int_0^{\infty} P_- \equiv \int_0^{\infty} [P_-(x) - 1] dx = 1.65 \pm 0.13 \quad (16)$$

from a number of different critical binary liquid mixtures.

In a later paper [22], Smith *et al.* considered the whole temperature range, including very close to the critical temperature, by numerically solving Maxwell's equations for a particular model for the universal scaling function $P_{\pm}(x)$. They demonstrated that both the RG [11] and MC [12] scaling functions provide a reasonable qualitative description of the $\bar{\rho}(t)$ data for four different critical binary liquid mixtures with the MC scaling function providing the more accurate representation. In the same publication they demonstrated that the ellipticity from critical adsorption can be reduced to a universal curve if the normalized value $\bar{\rho}_N = (\bar{\rho} - \bar{\rho}_{\text{BG}})/(\bar{\rho} - \bar{\rho}_{\text{BG}})_{\text{peak}}$ is plotted against the correlation length ξ (rather than the reduced temperature t). Here $(\bar{\rho} - \bar{\rho}_{\text{BG}})_{\text{peak}}$ is the peak value of $\bar{\rho} - \bar{\rho}_{\text{BG}}$ in the one-phase region. They found that the peak in $\bar{\rho}$, where $\bar{\rho}_N = 1$, occurred for a ξ_+/λ value of [40]

$$(\xi_+/\lambda)_{\text{peak}} = 0.064 \pm 0.006 \quad (17)$$

for four different liquid mixtures where $(\xi_+/\lambda)_{\text{peak}}$ is primarily determined by the ratio $c_+/P_{\infty+}$. The RG, MC, and Liu-Fisher ‘‘power-law-exponential’’ models enabled them to deduce that [40]

$$c_+/P_{\infty+} = 0.75 \pm 0.17 \quad (18)$$

for $(\xi_+/\lambda)_{\text{peak}}$ given by Eq. (17). [Note that the value of $c_+/P_{\infty+}$ depends slightly upon the model used (see the Appendix) and therefore Eq. (18) provides only a good estimate of this ‘‘universal’’ ratio.]

IV. THEORETICAL MODELS FOR THE CRITICAL ADSORPTION SCALING FUNCTION

In this section we consider a number of surface scaling functions which closely mimic the theoretical predictions given in Sec. II, while in the following section we use experimental measurements to determine the remaining parameters in these functions. Before we describe various models for $P_{\pm}(x)$, we first discuss the ‘‘vapor’’ side of the interface ($z < 0$). This ‘‘noncritical’’ portion of the model for $\varepsilon(z, t)$ does not depend upon the model that we use for $P_{\pm}(x)$. Following [39], we assume that the optical dielectric profile

$$\varepsilon(z, t) = 1 + \frac{[\varepsilon(0, t) - 1][1 + e^{-z/\xi_v}]}{1 + e^{-(z+z_e)/\xi_v}}, \quad z \leq 0, \quad (19)$$

where ξ_v is the noncritical vapor correlation length and the extrapolation length

$$z_e = \xi_{0\pm} \left(\frac{\varphi_L(0, t) - \varphi_L(+\infty, 0)}{M - c_{\pm}} \right)^{-\nu/\beta}. \quad (20)$$

For complete saturation by the L component, $\varphi_L(0, t) = 1$ and therefore the surface optical dielectric constant $\varepsilon(0, t) = \varepsilon_L$ in Eq. (19). For a given liquid and model for P_{\pm} , the only unknown parameter in Eqs. (19) and (20) is the vapor correlation length ξ_v . Smith *et al.* [22] used Eqs. (19) and (20) in their discussions of the RG and MC models.

For the liquid side of the interface ($z \geq 0$) from Eqs. (2), (3), and (12), $\varepsilon(z, t)$, used in the integration of Maxwell’s equations, is defined once a model for P_{\pm} has been specified. In [24] we provided a preliminary discussion of the $P1$ model for P_{\pm} , which is so designated because the function chosen for $P_{\pm}(x)$ is continuous up to and including the first derivative with respect to x . In this model we assume that the expansion at small $x (< x_o)$ takes the form

$$P_{s\pm}(x) = c_{\pm} x^{-\beta/\nu} + c_{1\pm} x^{(1-\beta)/\nu} \quad (21)$$

in agreement with Eq. (8), while the expansion at large $x (\geq x_o)$ takes the form

$$P_{l\pm}(x) = P_{\pm}(\infty) + P_{\infty\pm} e^{-x} + P_{1\pm} e^{-2x} \quad (22)$$

in agreement with Eq. (10). These two expansions are matched in value and in the first derivative at $x = x_o$ giving rise to the four equations

$$P_{1\pm} = \left[\frac{c_{\pm} x_o^{-\beta/\nu}}{1-\beta} - P_{\infty\pm} e^{-x_o} \left(1 - \frac{\nu x_o}{1-\beta} \right) - P_{\pm}(\infty) \right] \times e^{2x_o} \left(1 + \frac{2\nu x_o}{1-\beta} \right)^{-1} \quad (23)$$

and

$$c_{1\pm} = x_o^{(\beta-1)/\nu} [P_{\infty\pm} e^{-x_o} + P_{1\pm} e^{-2x_o} - c_{\pm} x_o^{-\beta/\nu}]. \quad (24)$$

For simplicity the matching point x_o is assumed to be the same in both the one- and two-phase regions. (This restriction is examined later in this paper.) In this model for P_{\pm} there are nine parameters which must be determined, specifically c_{\pm} , $c_{1\pm}$, $P_{\infty\pm}$, $P_{1\pm}$, and x_o . These nine parameters

are constrained by eight constraints: five *necessary constraints* described by Eqs. (6), (23), and (24), which any reasonable model must obey, and three *experimental constraints* described by Eqs. (15), (16), and (18). The eight constraints leave a single adjustable parameter, x_o , in the function P_{\pm} . The application of these eight constraints is rather complicated and is described in more detail in the Appendix. For a specific x_o value and vapor correlation length ξ_v , the optical dielectric profile $\varepsilon(z, t)$ is completely determined for the $P1$ model and the ellipticity $\bar{\rho}_{P1}(t)$ can be calculated by numerically integrating Maxwell’s equations.

The optimal values for x_o and ξ_v can be determined by minimizing the standard deviation

$$\sigma_{\rho} = \left(\sum_{i=1}^N [\bar{\rho}_i(t) - \bar{\rho}_{P1}(t)]^2 / (N-n) \right)^{1/2}, \quad (25)$$

where $\bar{\rho}_i(t)$ represents the experimental data, N ($= 400$) is the total number of experimental data points for the four liquid mixtures measured by Smith and Law [21], and n ($= 5$) is the number of adjustable parameters: x_o and four values of ξ_v , one associated with each liquid mixture. In the next section, where this optimization is done, the minimum value of σ_{ρ} is denoted by σ_{ρ}^{\min} . It is important to emphasize that *shape changes* in $\bar{\rho}_{P1}(t)$ only enter through the universal parameter x_o ; the parameter ξ_v merely moves a particular liquid mixture $\bar{\rho}_{P1}(t)$ curve vertically by a constant amount. This computational scheme is efficient in separating critical and noncritical effects. It provides a useful measure (σ_{ρ}^{\min}) for comparing different models for P_{\pm} .

The $P1$ model can systematically be improved by considering additional terms in the asymptotic expansions Eqs. (8) and (10) and requiring a corresponding number of higher derivatives of P_{\pm} to be continuous at x_o , so that x_o continues to be the sole adjustable parameter for P_{\pm} . Improvements in the $P1$ model may be important for physical phenomena which couple to higher-order derivatives of P_{\pm} [41]; for example, there is experimental evidence that the orientational order of dipolar molecules at surfaces may couple under certain circumstances to the second derivative of the local order parameter $m(z, t)$ [42,43]. In the next section we consider the $P3$ model where P_{\pm} is continuous up to and including the third derivative with respect to x . In the $P3$ model the small x expansion includes terms up to and including the $x^{(2-\beta)/\nu}$ term in Eq. (8), while the large x expansion includes terms up to and including the e^{-3x} term in Eq. (10). The small and large x expansions are matched up to and including the third derivative at the point x_o . There are thirteen parameters in the $P3$ model, namely c_{\pm} , $c_{1\pm}$, $c_{2\pm}$, $P_{\infty\pm}$, $P_{1\pm}$, $P_{2\pm}$, and x_o . Nine of these parameters are determined by the necessary (continuity) constraints, three more parameters are determined by the experimental constraints [Eqs. (15), (16), and (18)], while the last parameter x_o is determined by minimizing Eq. (25) as in the $P1$ model.

The final model that we consider in the next section is the ‘‘exponential-Pad e’’ (EP) profile

$$P_{+}(x) = c_{+} \left[\frac{1}{1 - e^{-x}} + \left(\frac{c_{+}}{P_{\infty+}} \right)^{-\nu/\beta} \right]^{\beta/\nu} e^{-x} \quad (26)$$

suggested by Liu and Fisher [10] to describe the crossover region between small and large x . This model is only valid in the one-phase region and conforms with Eqs. (4), (5), and (7).

V. ANALYSIS OF VARIOUS CRITICAL ADSORPTION SCALING MODELS

Smith *et al.* [39,21,22] studied the four critical binary liquid mixtures aniline-cyclohexane (AC), isobutyric acid-water (IW), nitrobenzene-hexane (NH), and 2,6-lutidine-water (LW). The first three liquid mixtures possess upper consolute points while the fourth mixture possesses a lower consolute point. All of these mixtures obey the condition $\sigma_L \ll \sigma_H$, where σ_i is the surface tension of the lighter (L) or heavier (H) liquid component; consequently the liquid/vapor surface is saturated with the lighter component to a good approximation, in both the one- and two-phase regions [21]. We are therefore in the completely saturated regime where the universal surface scaling function P_{\pm} [Eq. (3)] is appropriate in describing the adsorption structure. Smith and Law [21] demonstrated that capillary wave fluctuations essentially add a constant amount to the ellipticity $\bar{\rho}(t)$; this contribution is effectively taken into account therefore by the vapor correlation length ξ_v [which appears in Eq. (19)] because ξ_v has an identical effect on $\bar{\rho}(t)$. The experimental $\bar{\rho}(t)$ data for these four liquid mixtures is provided in [21]. In all of these measurements, the transverse thermal gradients were less than ~ 1 mK/cm and a sufficiently long time (typically 4 to 6 h) was allowed for the system to come into thermal and diffusive equilibrium at each temperature where at the end of this waiting period the thermal stability was typically ± 1 mK over 4 h, while at each reduced temperature t twenty $\bar{\rho}(t)$ measurements were collected and averaged over a period of 1 h. From this data set, Smith *et al.* measured the universal integrals $\int P_+$ [Eq. (15)], $\int P_-$ [Eq. (16)] [39,21], and the universal ratio $c_+/P_{\infty+}$ [Eq. (18)] [22,24]. In this section we compare the $P1$, $P3$, and EP scaling function models, suggested in the preceding section, with the experimental data set for the four liquid mixtures.

A. $P1$ model

We first consider the case where the ratio of the correlation length amplitudes $R_{\xi} = \xi_{0+}/\xi_{0-} = 1.96$. In Fig. 1 we show the variation of $\bar{\rho}_{P1}(t)$ calculated for the AC mixture for different values of x_o . The behavior at large $t \geq 10^{-3}$ in both the one- and two-phase regions is insensitive to the value of x_o and is determined by the universal numbers given in Eqs. (15) and (16), respectively. Additionally in the one-phase region the peak position always occurs at the same reduced temperature value, which is governed by Eq. (17), while Eq. (6) forces the one- and two-phase curves for each x_o to be continuous at $t=0$. The shape of $\bar{\rho}_{P1}(t)$ depends significantly upon x_o for small reduced temperatures $t \leq 10^{-3}$ in both phases. When the $P1$ model is minimized according to the scheme described in Sec. IV, the minimum standard deviation $\sigma_{\rho,P1}^{\min} = 1.3756 \times 10^{-4}$ occurs for $x_o = 1.15$. This optimal $P1$ model is displayed in Fig. 2 (dashed line), while its parameters are listed in Table I. In Fig. 3, the

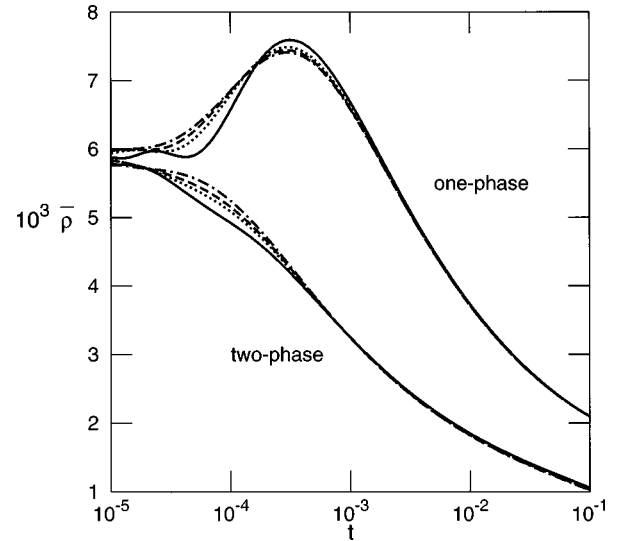


FIG. 1. Plot of $\bar{\rho}$ versus t for the $P1$ model with $R_{\xi} = 1.96$ in both the one- and two-phase regions. The curves are for differing values of $x_o = 0.7$ (dash-dotted line), 1.0 (dashed line), 1.2 (dotted line), and 1.6 (solid line).

$P1$ model (dashed line) is compared with the experimental data for the AC mixture. Comparisons with the other three mixtures are given in [24]. The $P1$ model provides an excellent description of all four mixtures in both the one- and two-phase regions. The experimental error for $\bar{\rho}(t)$, typically $\Delta \bar{\rho} \sim 5 \times 10^{-5}$, does not take into account effects due to the presence of any transverse thermal gradients and uncertainties in the critical temperature, critical composition, correlation length amplitude ξ_{o+} , and coexistence curve amplitude M_- , etc. The real error associated with each $\bar{\rho}(t)$ point should be larger than $\Delta \bar{\rho}$. We believe that $\sigma_{\rho,P1}^{\min}$ provides a more accurate description of the true errors in $\bar{\rho}(t)$ for a

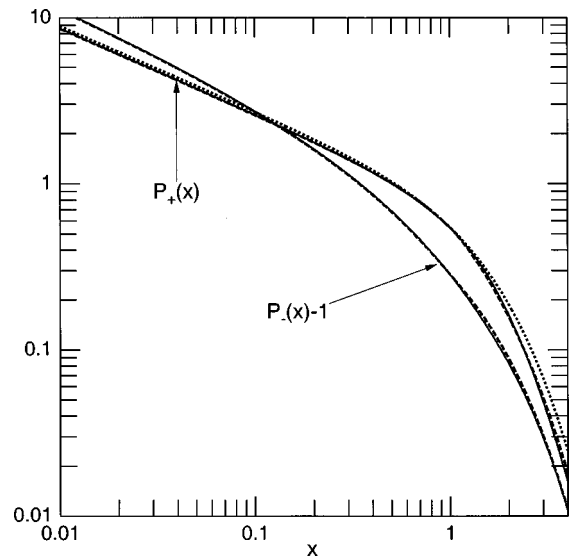


FIG. 2. Plot of the universal critical adsorption scaling functions $P_+(x)$ and $P_-(x) - 1$ versus x for different models: $P1$ (dashed line), $P3$ (solid line), and EP model (dotted line). In this figure the $P1$ and $P1a$ models are indistinguishable; similarly, the $P3$ and $P3a$ models are indistinguishable.

TABLE I. Critical adsorption scaling function models. (Note: the $P1$ model below corrects some minor errors in [24].)

Model	Phase	$x_{o\pm}$	c_{\pm}	$c_{1\pm}$	$c_{2\pm}$	$P_{\infty\pm}$	$P_{1\pm}$	$P_{2\pm}$	$10^4 \sigma_{\rho}^{\min}$
$P1$	1	1.15	$0.788^{+0.009}_{-0.015}$	-0.245		$0.963^{+0.117}_{-0.201}$	1.437		1.3756
	2	1.15	$1.117^{+0.013}_{-0.021}$	0.169		$0.572^{+0.357}_{-0.152}$	0.533		
$P1a$	1	1.15	0.788	-0.245		0.963	1.437		1.3757
	2	1.15	1.047	0.185		0.433	0.516		
$P3$	1	1.60	0.791	-0.284	0.032	0.809	3.469	-4.852	1.4476
	2	1.60	1.122	0.170	-0.0091	0.590	-0.109	1.661	
$P3a$	1	1.57	0.792	-0.286	0.033	0.826	3.266	-4.394	1.4481
	2	0.86	1.123	0.148	0.0051	0.659	-0.515	2.076	
EP	1		0.817			1.035			1.5492

carefully prepared critical binary liquid mixture, assuming that the $P1$ model is a good representation of the actual scaling functions. In [24], $\sigma_{\rho, P1}^{\min}$ was assumed to represent the true experimental error associated with each $\bar{\rho}(t)$ data point; 95% confidence levels were determined from the χ^2 distribution. For convenience these 95% confidence levels are also listed in Table I; if they were displayed in Fig. 2, they would barely be visible. The narrow region defined by the 95% confidence levels suggests that the true P_{\pm} function must lie within this narrow region in order to be able to explain the experimental $\bar{\rho}$ data for the four liquid mixtures.

The results in Fig. 1 suggest that perhaps a better fit could be obtained between theory and experimental data if separate crossover points, denoted x_{o+} and x_{o-} , were used in, respectively, the one- and two-phase regions. Such an extension will be considered later for the $P3$ model.

If $R_{\xi} = \xi_{0+}/\xi_{0-} = 1.73$ (rather than $R_{\xi} = 1.96$), as suggested by the calculations of Flöter and Dietrich [23], we find similar agreement between this model (denoted the $P1a$ model) and experimental data as indicated by a $\sigma_{\rho, P1a}^{\min} = 1.3757 \times 10^{-4}$. The parameters differ slightly for the $P1a$

model compared with the $P1$ model and are listed in Table I, however the shape for the $P1a$ model can barely be distinguished from the $P1$ model (Fig. 2, dashed line) and therefore it will provide a similar agreement with the experimental $\bar{\rho}$ data. This indicates that the $\bar{\rho}$ data cannot be used to differentiate between differing values for R_{ξ} . The ratios c_{1+}/c_{1-} and c_{2+}/c_{2-} [Eq. (9)], derived from the analyticity of the analytic background at $t=0$, provide an additional self-consistency test for the theoretical models. In Table II, we compare c_{1+}/c_{1-} for the $P1$ and $P1a$ models together with the theoretical expectations from Eq. (9). In both cases c_{1+}/c_{1-} is negative, as predicted by Eq. (9), however it is approximately $\sim 20-30\%$ lower than expectations.

B. $P3$ model

We have repeated the calculation for the $P3$ model with $R_{\xi} = 1.96$ (Fig. 2, solid line). For this model we find that $\sigma_{\rho, P3}^{\min} = 1.4476 \times 10^{-4}$ for $x_o = 1.60$, where the parameters are given in Table I and the comparison with experiment for the AC mixture is shown in Fig. 3 (solid line). Figure 2 demonstrates that there is very little difference between the optimal shapes for the $P1$ and $P3$ models. The $P3$ model will therefore provide the same quantitative agreement as the $P1$ model (which was displayed in [24]) with regards to the $\bar{\rho}(t)$ data for the other three liquid mixtures. In Table II we compare the ratios c_{1+}/c_{1-} and c_{2+}/c_{2-} for the $P3$ model with the predictions from Eq. (9).

In Fig. 1 (applicable for the $P1$ model) the curves suggest that a better description of the experimental data might be obtained if separate matching points x_{o+} and x_{o-} are used in, respectively, the one- and two-phase regions. We have modified the $P3$ model to allow for these two adjustable parameters. We call this modified $P3$ model the $P3a$ model. The use of two adjustable parameters involves considerably more work than for a single adjustable parameter x_o , be-

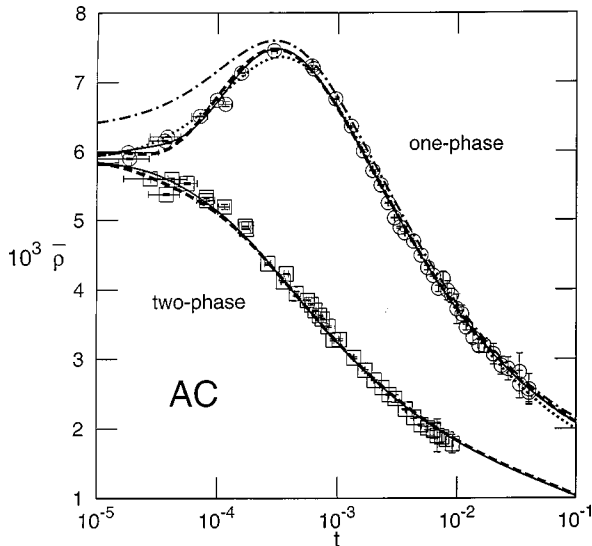


FIG. 3. Comparison of the various models with the experimental data (symbols) for the aniline-cyclohexane mixture: $P1$ (dashed line), $P3$ (solid line), EP constrained model (dash-dotted line, see text), and EP model (dotted line).

TABLE II. Critical adsorption amplitude ratios.

Model	c_{1+}/c_{1-}	$-R_{\xi}^{(1-\beta)/\nu}$	c_{2+}/c_{2-}	$+R_{\xi}^{(2-\beta)/\nu}$	R_{ξ}
$P1$	-1.45	-2.05			1.96
$P1a$	-1.32	-1.79			1.73
$P3$	-1.67	-2.05	-3.5	+5.93	1.96
$P3a$	-1.93	-2.05	+6.5	+5.93	1.96

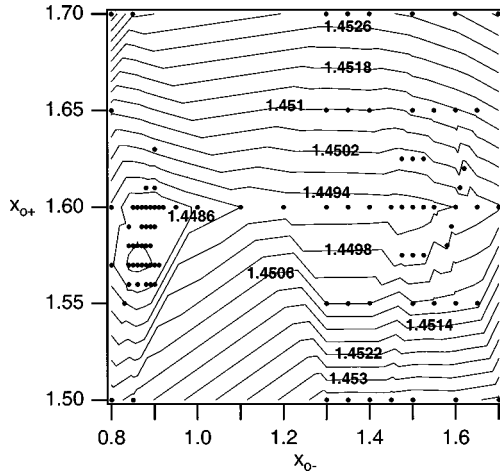


FIG. 4. Contour map of the variation in $10^4 \sigma_\rho$ for various values of (x_{o-}, x_{o+}) for the $P3a$ model where the solid circles indicate the specific points where calculations were conducted. The global minimum in σ_ρ occurs at $(x_{o-}^{\min}, x_{o+}^{\min}) = (0.86, 1.57)$, where $\sigma_{\rho, P3a}^{\min} = 1.4481 \times 10^{-4}$.

cause now a two-dimensional space must be searched for the global minimum in σ_ρ . It is difficult to fully automate our computational procedure, hence this search is conducted by selecting values for the pair (x_{o-}, x_{o+}) in the vicinity of our previous optimal value $x_o = 1.60$ and then calculating σ_ρ . Figure 4 shows a plot of the function $\sigma_\rho(x_{o-}, x_{o+})$ where the global minimum for σ_ρ has a value of $\sigma_{\rho, P3a}^{\min} = 1.4481 \times 10^{-4}$ at $(x_{o-}^{\min}, x_{o+}^{\min}) = (0.86, 1.57)$. We note that the function $\sigma_\rho(x_{o-}, x_{o+})$ is extremely flat and relatively insensitive to the precise value of (x_{o-}, x_{o+}) ; this function exhibits a very shallow minimum where $\sigma_{\rho, P3a}^{\min}$ is only one part in 1800 smaller than the value of σ_ρ at $(x_{o-}, x_{o+}) = (1.60, 1.60)$. In the $P3a$ model, $x_{o+}^{\min} = 1.57$ is still quite close to the value of $x_o = 1.60$ for the $P3$ model, however $x_{o-}^{\min} = 0.86$ differs considerably from this value. The parameters for the $P3a$ model are listed in Table I while the shape for this model is essentially indistinguishable from the $P3$ model in Fig. 2 (solid line). [Note that in Table I, $\sigma_{\rho, P3a}^{\min} = 1.4481 \times 10^{-4}$ is slightly larger than $\sigma_{\rho, P3}^{\min} = 1.4476 \times 10^{-4}$ even though one has one additional adjustable parameter for the $P3a$ model; this is because the number of degrees of freedom $N-n$ which occurs in the formula for σ_ρ is slightly smaller for the $P3a$ model ($N-n=394$) than for the $P3$ model ($N-n=395$).] In Table II we compare the ratios c_{1+}/c_{1-} and c_{2+}/c_{2-} with the theoretical expectations from Eq. (9). Of all of the models considered, the $P3a$ model provides the most consistent agreement with theoretical predictions for these ratios, however this agreement comes at a considerable cost in extra effort for only a marginal change in the shape of $P_\pm(x)$.

C. EP model

For the EP model (which can only be applied in the one-phase region), if we require that both of the experimental constraints given in Eqs. (15) and (18) hold, then the parameters c_+ and $P_{\infty+}$ are determined and this model is completely constrained, thus providing no degree of freedom with which to improve the agreement between this model

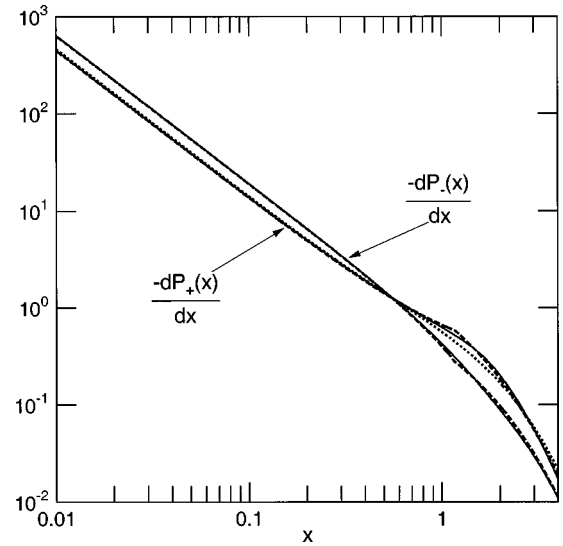


FIG. 5. Graph of dP_\pm/dx versus x for the models $P1$ (dashed line), $P3$ (solid line), and EP (dotted line).

and experiment. Good agreement is not obtained between this model and experimental data (Fig. 3, dash-dotted line), especially at small reduced temperatures t . The ratio $c_+/P_{\infty+}$ has a rather large experimental error bar associated with it, therefore if we loosen the restriction that Eq. (18) must hold, then much better agreement is found between the EP model and experiment (Fig. 3, dotted line). The best fit occurs for $\sigma_{\rho, EP}^{\min} = 1.5492 \times 10^{-4}$, where the parameters for this model are given in Table I. The larger standard deviation $\sigma_{\rho, EP}^{\min}$ for the EP model indicates that the $P1$ and $P3$ models provide a slightly better description of the experimental data.

D. Derivatives

Molecules may orient at the liquid-vapor surface for many differing reasons. If the molecules are amphiphilic so that one end of the molecule prefers to be oriented towards the vapor side while the other end of the molecule prefers to be oriented towards the liquid side of the interface, then it has been suggested [41] that this orientational order couples to the first derivative of the order-parameter profile. If, however, the molecule is dipolar, then the orientational order couples to the second derivative [44,41,45], or perhaps to the first derivative squared [45], of the order-parameter profile [46]. In [42,43] we have found experimental evidence that for highly polar molecules the orientational order couples to the second derivative of the order parameter, at least at the critical liquid/liquid interface of critical binary liquid mixtures. There seems to be no physical reason why such concepts should not also apply at the noncritical liquid/vapor interface of critical binary liquid mixtures where the order parameter is described by the universal function $P_\pm(x)$ of Eq. (3). In Figs. 5 and 6 we therefore display $P'_\pm(x)$ and $P''_\pm(x)$, respectively, where the prime refers to differentiation with respect to x . The derivatives for the $P1$ (dashed line), $P3$ (solid line), and EP (dotted line) models are similar in shape and value except that the $P1$ model displays a discontinuity in its second derivative as expected. These similarities between the various models suggest that they probably provide a reasonable estimate for the true derivatives of the P_\pm function.

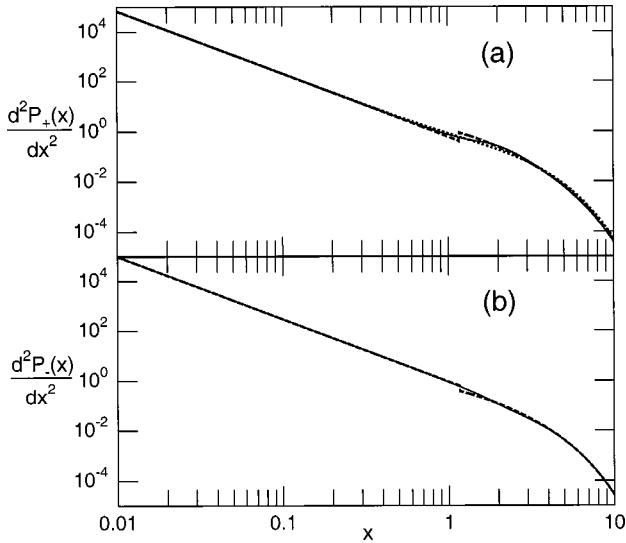


FIG. 6. Graph of $d^2 P_{\pm}/dx^2$ versus x for the models $P1$ (dashed line), $P3$ (solid line), and EP (dotted line) in the (a) one- and (b) two-phase regions.

VI. SUMMARY AND DISCUSSION

In this paper we have extended an earlier study [24] of critical adsorption at the noncritical liquid/vapor surface of critical binary liquid mixtures in the limit of strong saturation of one of the liquid components. Under such conditions the critical adsorption profile is described by a universal scaling function $P_{\pm} \equiv P_{\pm}(x)$, which takes a differing form in the one- (+) and two- (-) phase region where the dimensionless length $x = z/\xi_{\pm}$ and ξ is the correlation length. P_{\pm} possesses well-known asymptotic forms at small and large x [Eqs. (8) and (10)]. By considering various experimental constraints and continuity constraints in the dimensionless length x and reduced temperature t , we have constructed two models, $P1$ and $P3$, which are continuous up to and including, respectively, the first and the third derivatives of x . $P1$ and $P3$ possess only one adjustable parameter x_o , the matching point where the small x behavior is matched to the large x behavior. The parameter x_o is adjusted to provide the best agreement with the experimental ellipsometric measurements ($\bar{\rho}$) from four different critical liquid mixtures. These models, which are listed in Table I, provide an excellent description of the experiments (Fig. 3) with an acceptably small standard deviation σ_{ρ}^{\min} . In the analysis, each model is compared with all four critical liquid mixtures, however for simplicity the agreement for each model is only directly displayed for the critical liquid mixture aniline + cyclohexane (Fig. 3). The other three liquid mixtures exhibit a similar level of agreement/disagreement with each model. A comparison between the $P1$ model and all four mixtures is provided in [24].

The ratio of the correlation length amplitudes $R_{\xi} = \xi_{o+}/\xi_{o-}$ occurs within the $P1$ and $P3$ models. A number of differing values for R_{ξ} have been proposed for the “true correlation length” amplitude ratio [23], however the shape that we deduce for the P_{\pm} function using our minimization scheme is relatively insensitive to the value assumed for R_{ξ} , for example the $P1$ model (where $R_{\xi} = 1.96$) and the $P1a$ model (where $R_{\xi} = 1.73$) have similar standard deviations

σ_{ρ}^{\min} (Table I). We have also examined whether or not a better description of the experimental data could be obtained using differing matching points in the one- (x_{o+}) and two- (x_{o-}) phase regions, the $P3a$ model (with $R_{\xi} = 1.96$). This more complicated model requires considerably more effort to determine. It exhibits only a marginal change in shape for $P_{\pm}(x)$ compared with the $P3$ model (Fig. 2), however it provides very good consistency (Table II) for the ratios c_{1+}/c_{1-} and c_{2+}/c_{2-} compared with Eq. (9) derived from the analyticity of the analytic background at $t=0$.

The “universal” amplitudes which occur in each model are listed in Table I. These amplitudes are relatively independent of the model considered with the exception of P_{1+} and P_{1-} , which differ significantly between the $P1$ and $P3$ models. We believe that this effect is due to the strong correlation between the parameter x_o [$=1.15$ (1.60) for the $P1$ ($P3$) model] and the magnitudes of the parameters $P_{1\pm}$ and $P_{2\pm}$ determined by the continuity conditions at x_o [Eqs. (23) and (24)]. The $P1$ and $P3$ models differ primarily at large $x \approx 2$ (Fig. 2), where the terms $P_{1\pm}e^{-2x}$ and $P_{2\pm}e^{-3x}$ which appear in the large x expansion [Eq. (10)] will be much smaller than the leading-order term $P_{\infty\pm}e^{-x}$; consequently, the amplitudes $P_{1\pm}$ and $P_{2\pm}$ will be determined with less certainty. Additionally, Fig. 4 indicates that our experimental measurements are not particularly sensitive to the precise value for x_o , hence changes in x_o will only lead to a marginal change in σ_{ρ} but can generate significant changes in the magnitudes of the parameters $P_{1\pm}$ and $P_{2\pm}$. To a very good approximation, the optimal $P_{\pm}(x)$ function derived from the $P1$ and $P3$ models (including their variants $P1a$ and $P3a$) generates the *same universal shape* for the critical adsorption surface scaling function (Fig. 2). The narrow 95% confidence region displayed by the $P1$ model, which would barely be visible in Fig. 2, indicates that even small deviations from this universal shape will lead to measurable discrepancies between a model and the experimental $\bar{\rho}$ data. We believe that the *most* important concept resulting from this paper is the *universal shape* for the $P_{\pm}(x)$ function exhibited in Fig. 2. This shape can be parametrized in various ways. The $P1$ and $P3$ models, in this paper, provide good examples of such a parametrization. Different parametrizations will naturally lead to different amplitudes within each model; our contention is that although these amplitudes within individual models are important, they are of secondary importance to the universal shape for the $P_{\pm}(x)$ function. Theoretical determinations of $P_{\pm}(x)$ should therefore be compared with this universal shape rather than with specific amplitudes, whose value will be somewhat model dependent. If theory is to be compared with specific amplitudes then the model most consistent with theoretical expectations is the $P3a$ model, which provides agreement with Eq. (9).

We have also considered the exponential-Padé (EP) model of Liu and Fisher [10], which asymptotically possesses the predicted theoretical dependence at small and large x . This model provides a reasonable but less accurate description of the one-phase ellipsometric $\bar{\rho}$ data, however it has the advantage that it is continuous in all derivatives. The $P_{+}(x)$ surface scaling function derived from this model is quantitatively very similar to the $P1$ and $P3$ models (Fig. 2).

This research work has been supported by the National Science Foundation through Grant No. DMR-9631133.

APPENDIX

In this appendix, we describe how to apply both the necessary and experimental constraints to the $P1$ and $P3$ models. In the $P1$ model there are nine parameters. The five necessary constraints, Eqs. (6), (23), and (24), allow the parameters $c_{1\pm}$, $P_{1\pm}$, and c_- to be expressed in terms of the four parameters c_+ , $P_{\infty\pm}$, and x_o . We initially select a value of x_o (close to 1), use Eq. (18) to determine $P_{\infty+}$ in terms of c_+ in $P_+(x)$, and finally an integration of $P_+(x)$ determines c_+ from Eq. (15). Similarly, an integration of $P_-(x)$ determines $P_{\infty-}$ according to Eq. (16). The value of x_o is incremented/decremented and the calculation is repeated until the standard deviation σ_ρ , as computed by Eq. (25), is a minimum. The noncritical correlation lengths ξ_v , which appear in Eq. (19), are also adjusted to minimize σ_ρ .

This procedure, although long and tedious, would be relatively straightforward if not for the fact that the ratio $c_+/P_{\infty+}$ is somewhat model dependent, as previously noted by Smith *et al.* [22], and therefore Eq. (18) only provides an estimate for this ratio. This complicates the above calculation because we have to redetermine the ratio $c_+/P_{\infty+}$ for each value of x_o . This is accomplished by following the procedure in [22]. For a particular value of x_o we select four values of $c_+/P_{\infty+}$, compute the theoretical $\bar{\rho}(t)$ curves for all four liquid mixtures, and then from each of these curves determine $(\xi_+/\lambda)_{\text{peak}}$. These $(\xi_+/\lambda)_{\text{peak}}$ values are then plotted against the $c_+/P_{\infty+}$ ratios. A linear regression through these theoretical data determines the value of $c_+/P_{\infty+}$ (for this value of x_o) corresponding to the experimental value of $(\xi_+/\lambda)_{\text{peak}}$ given in Eq. (17). We show an example of this calculation in Fig. 7. The symbols correspond to the theoretically computed $(\xi_+/\lambda)_{\text{peak}}$ values for various values of $c_+/P_{\infty+}$ for $x_o=1.0$ (circles) and $x_o=1.1$ (solid circles). The solid lines are linear regressions to these theoretical data, the RG data (solid squares), and the MC data (solid triangles) for $x_o=1.0$ (light line) and $x_o=1.1$ (heavy line). The intersections between the solid lines and the experimental value [Eq. (17), Fig. 7, horizontal dashed line] provide the optimal values for $c_+/P_{\infty+}$. From

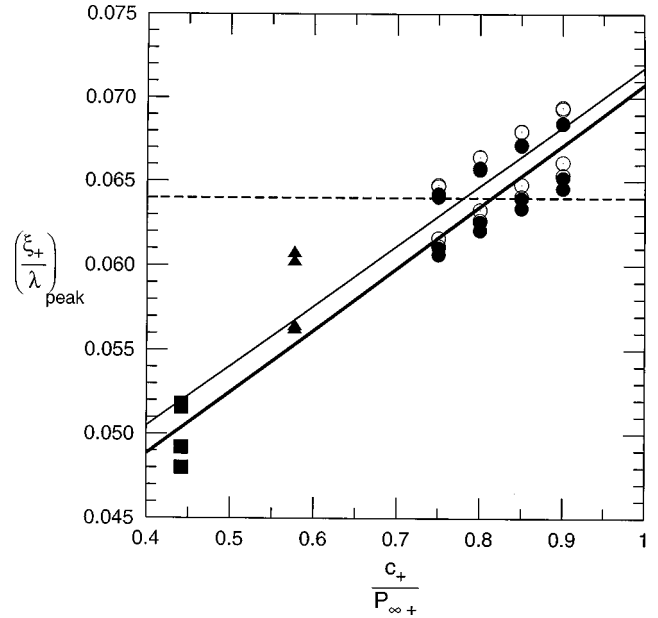


FIG. 7. Example demonstrating how the ratio $c_+/P_{\infty+}$ is determined for a particular model and value of the matching parameter x_o . The circles represent the $P1$ model with $x_o=1.0$ (open circles) and $x_o=1.1$ (solid circles), the RG model (solid squares), and the MC model (solid triangles) for the four liquid mixtures. The solid lines are linear regression fits to the RG, MC, and either $x_o=1.0$ (light line) or $x_o=1.1$ (heavy line) data. The intersection between a solid line and the horizontal dashed line [Eq. (17)] provides the $c_+/P_{\infty+}$ value for a given x_o value.

Fig. 7, $c_+/P_{\infty+}=0.78$ for $x_o=1.0$ and $c_+/P_{\infty+}=0.81$ for $x_o=1.1$. It is these values of $c_+/P_{\infty+}$ for given x_o which are used in the $P1$ procedure above, rather than the value given in Eq. (18).

An identical procedure is used to determine the $P3$ model; however, in this case we have 13 parameters. The eight linear equations associated with the continuity constraints applied at x_o , together with Eq. (6), enable the nine parameters $c_{1\pm}$, $c_{2\pm}$, $P_{1\pm}$, $P_{2\pm}$, and c_- to be determined from values for c_+ , $P_{\infty\pm}$, and x_o . After this step, the procedure for determining the $P3$ model is identical to that used for the $P1$ model.

-
- [1] B. M. Law, Phys. Rev. E **48**, 2760 (1993).
 [2] J.-M. Petit, B. M. Law, and D. Beysens, J. Colloid Interface Sci. **202**, 441 (1998); B. M. Law, J.-M. Petit, and D. Beysens, Phys. Rev. E **57**, 5782 (1998).
 [3] V. Ganesan and H. Brenner, Phys. Rev. Lett. **81**, 578 (1998).
 [4] M. E. Fisher and P.-G. de Gennes, C. R. Seances Acad. Sci., Ser. B **287**, 207 (1978).
 [5] M. E. Fisher and J.-H. Chen, J. Phys. (Paris) **46**, 1645 (1985).
 [6] H. W. Diehl, in *Phase Transitions and Critical Phenomena*, edited by C. Domb and J. L. Lebowitz (Academic, London, 1986), Vol. 10.
 [7] A. Kumar, H. R. Krishnamurthy, and E. S. R. Gopal, Phys. Rep. **98**, 57 (1983).
 [8] U. Ritschel and P. Czerner, Phys. Rev. Lett. **77**, 3645 (1996); P. Czerner and U. Ritschel, Physica A **237**, 240 (1997); A. Ciach and U. Ritschel, Nucl. Phys. B **489**, 653 (1997); A. Ciach, A. Maciolek, and J. Stecki, J. Chem. Phys. **108**, 5913 (1998).
 [9] N. S. Desai, S. Peach, and C. Franck, Phys. Rev. E **52**, 4129 (1995).
 [10] A. J. Liu and M. E. Fisher, Phys. Rev. A **40**, 7202 (1989).
 [11] H. W. Diehl and M. Smock, Phys. Rev. B **47**, 5841 (1993); **48**, 6470(E) (1993).
 [12] M. Smock, H. W. Diehl, and D. P. Landau, Ber. Bunsenges. Phys. Chem. **98**, 486 (1994).
 [13] S. Blümel and G. H. Findenegg, Phys. Rev. Lett. **54**, 447 (1985).
 [14] D. Beysens and S. Leibler, J. Phys. (France) Lett. **43**, L133 (1982).

- [15] C. Franck and S. E. Schnatterly, *Phys. Rev. Lett.* **48**, 763 (1982); J. A. Dixon, M. Schlossman, X.-L. Wu, and C. Franck, *Phys. Rev. B* **31**, 1509 (1985); M. Schlossman, X. L. Wu, and C. Franck, *ibid.* **31**, 1478 (1985).
- [16] D. Beaglehole, *J. Chem. Phys.* **73**, 3366 (1980); **75**, 1544 (1981); *Phys. Lett.* **91A**, 237 (1982); *J. Phys. Chem.* **87**, 4749 (1983).
- [17] B. Heidel and G. H. Findenegg, *J. Phys. Chem.* **88**, 6575 (1984); *J. Chem. Phys.* **87**, 706 (1987).
- [18] J. W. Schmidt and M. R. Moldover, *J. Chem. Phys.* **83**, 1829 (1985); J. W. Schmidt, *ibid.* **85**, 3631 (1986).
- [19] H. Zhao, A. Penninckx-Sans, L.-T. Lee, D. Beysens, and G. Jannink, *Phys. Rev. Lett.* **75**, 1977 (1995).
- [20] J. R. Howse, J. Bowers, E. Manzanares-Papayanopoulos, I. A. McLure, and R. Steitz, *Phys. Rev. E* **59**, 5577 (1999).
- [21] D. S. P. Smith and B. M. Law, *Phys. Rev. E* **54**, 2727 (1996).
- [22] D. S. P. Smith, B. M. Law, M. Smock, and D. P. Landau, *Phys. Rev. E* **55**, 620 (1997).
- [23] G. Flóter and S. Dietrich, *Z. Phys. B: Condens. Matter* **97**, 213 (1995).
- [24] J. H. Carpenter, B. M. Law, and D. S. P. Smith, *Phys. Rev. E* **59**, 5655 (1999).
- [25] M. Krech, *The Casimir Effect in Critical Systems* (World Scientific, Singapore, 1994), and references therein.
- [26] S. Gnutzmann and U. Ritschel, *Z. Phys. B: Condens. Matter* **96**, 391 (1995).
- [27] H. B. Tarko and M. E. Fisher, *Phys. Rev. Lett.* **31**, 926 (1973).
- [28] A. J. Liu and M. E. Fisher, *Physica A* **156**, 35 (1989).
- [29] C. Ruge, P. Zhu, and F. Wagner, *Physica A* **209**, 431 (1994).
- [30] T. W. Burkhardt and H. W. Diehl, *Phys. Rev. B* **50**, 3894 (1994).
- [31] Note that the ratio c_{2+}/c_{2-} [Eq. (9)] corrects a sign error in the corresponding expression in [11].
- [32] D. Beaglehole, in *Fluid Interfacial Phenomena*, edited by C. A. Croxton (Wiley, New York, 1986).
- [33] V. L. Kuzmin and V. P. Romanov, *Phys. Rev. E* **49**, 2949 (1994).
- [34] J. Lekner, *Theory of Reflection* (Martinus Nijhoff, Dordrecht, 1987).
- [35] P. K. L. Drude, *The Theory of Optics* (Dover, New York, 1959), p. 292.
- [36] B. M. Law and D. Beaglehole, *J. Phys. D* **14**, 115 (1981).
- [37] M. Born and E. Wolf, *Principle of Optics* (Pergamon, Oxford, 1980), Sec. 1.6.
- [38] R. F. Kayser, *Phys. Rev. B* **34**, 3254 (1986).
- [39] D. S. P. Smith and B. M. Law, *Phys. Rev. E* **52**, 580 (1995).
- [40] The values given in Eqs. (17) and (18) are from [24] deduced using the procedure given in [22].
- [41] B. Widom, *J. Phys. Chem.* **100**, 13 190 (1996).
- [42] C. L. Caylor, B. M. Law, P. Senanayake, V. L. Kuzmin, V. P. Romanov, and S. Wiegand, *Phys. Rev. E* **56**, 4441 (1997).
- [43] A. Mukhopadhyay, C. L. Caylor, and B. M. Law (unpublished).
- [44] T. J. Sluckin, *Mol. Phys.* **47**, 267 (1982); **43**, 817 (1981).
- [45] J.-P. Carton and L. Leibler, *J. Phys. (France)* **51**, 1683 (1990).
- [46] Note that Widom [41] uses a slightly different terminology from that used here. In our terminology, dipolar molecules possess a permanent dipole moment without any amphiphilic properties; thus a particular end of the molecule has no preference for being in a particular phase. Widom calls such molecules nematic. Our amphiphilic molecules whose ends possess a preference for being in a particular phase are called dipolar by Widom.